Proximate Dirac spin liquid in the honeycomb lattice math xmlns="http://www.w3.org/1998/Math/MathML">mrow>msub>mi>J/mi>mn>1/mn>/msub>mtext>−/mtext>msub>mi>J/mi>mn>3/mn>/msub>/mrow>/math> XXZ model: Numerical study and application to cobaltates

Anjishnu Bose, Manodip Routh, Sreekar Voleti, Sudip Kumar Saha, Manoranjan Kumar, Tanusri Saha-Dasgupta, and Arun Paramekanti

Phys. Rev. B **108**, 174422 — Published 16 November 2023

DOI: 10.1103/PhysRevB.108.174422

Proximate Dirac spin liquid in honeycomb lattice J_1-J_3 XXZ model: Numerical study and application to cobaltates

Anjishnu Bose,[1,*] Manodip Routh,[2,*] Sreekar Voleti,[1,*] Sudip Kumar Saha,[2]
Manoranjan Kumar,[2] Tanusri Saha-Dasgupta,[2] and Arun Paramekanti[1,2,3]

[1] *Department of Physics, University of Toronto, 60 St. George Street, Toronto, ON, M5S 1A7 Canada*
[2] *Department of Condensed Matter Physics and Materials Science, S.N. Bose National Centre for Basic Sciences, Kolkata 700098, India.*
[3] *International Centre for Theoretical Sciences, Bengaluru 560089, India*

(Dated: November 2, 2023)

Recent theoretical and experimental work suggest that the honeycomb cobaltates, initially proposed as candidate Kitaev quantum magnets, are in fact described by a pseudospin-1/2 easy-plane spin Hamiltonian with nearest neighbor ferromagnetic (FM) exchange J_1 being frustrated by antiferromagnetic third-neighbor exchange J_3 and weaker compass anisotropies. Using exact diagonalization and density-matrix renormalization group (DMRG) calculations, we show that this model exhibits FM order at small J_3/J_1 and zig-zag (ZZ) order at large J_3/J_1, separated by an intermediate phase, which we label as $\widetilde{\text{SL}}$. This $\widetilde{\text{SL}}$ phase is shown to exhibit spin-liquid-like correlations in DMRG, although we cannot preclude weak broken symmetries, e.g. weak Ising type Néel order, given the limits on our explored system sizes. Using a modified parton mean field theory and variational Monte Carlo on Gutzwiller projected wavefunctions, we show that the optimal FM and ZZ orders as well as the intermediate $\widetilde{\text{SL}}$ state are proximate to a 'parent' Dirac spin liquid (SL). This Dirac SL is shown to capture the broad continuum in the temperature and magnetic field dependent terahertz spectroscopy of $BaCo_2(AsO_4)_2$, and the reported low temperature metallic thermal conductivity in $Na_2Co_2TeO_6$ and $BaCo_2(AsO_4)_2$ upon incorporating disorder induced broadening.

Quantum spin liquids (SLs) are exotic magnetic liquids featuring fluctuating singlet correlations and fractionalized spin excitations, which may be fruitfully described using the language of gauge-matter theories [1–5]. While initially proposed as interesting magnetic ground states formed by a quantum superposition of a large number of classically frustrated spin or singlet dimer configurations [6, 7], interest in SLs exploded with the idea that doping such insulators might lead to high temperature superconductivity [8, 9]. For gapped SLs, their robust topological order [1] and the absence of local order parameters in SLs has also rendered them as platforms of potential interest for topologically protected quantum memories [10].

The search for quantum SLs has unearthed several promising candidates in materials with strong geometric frustration such as kagomé [11–15], hyperkagomé [16–18], and pyrochlore [19–22] magnets, as well as in quantum simulators using Rydberg atoms [23]. A significant effort has also been devoted to exploring the physics of the exactly solvable Kitaev quantum SL with Majorana excitations [10, 24, 25] in pseudospin-1/2 honeycomb magnets such as iridates [26–29], α-$RuCl_3$ [30–32], and their higher spin generalizations [33, 34]. While many of these quantum magnets have ordered ground states, their dynamical response is nevertheless expected to provide a window into SL physics at intermediate energy scales.

Recently, it was proposed that the honeycomb cobaltates, with d^7 Co^{2+} ions in an octahedral crystal field environment, provide an alternative venue to realize the Kitaev model [35, 36]. This has led to a large body of experimental work on a variety of these materials including $BaCo_2(AsO_4)_2$ [37–42], $BaCo_2(PO_4)_2$ [43], $Na_2Co_2TeO_6$ [44–48], and $Na_3Co_2SbO_6$ [45, 49]. While most of these cobaltates display collinear or spiral magnetic ground states [37–41, 43, 50–52], or proposed triple-Q orders [53], there are tantalizing signatures in $BaCo_2(AsO_4)_2$ of a spin-liquid-like broad continuum in the terahertz (THz) response [40]. Experiments on $Na_2Co_2TeO_6$ and $BaCo_2(AsO_4)_2$ have also reported a residual metallic thermal conductivity $\kappa \propto T$ [42, 48] which hints at mobile fermionic spinons; however, phonon contributions to $\kappa(T)$ remain to be understood [54].

The THz and thermal conductivity results suggest that although the ground state of the cobaltates might exhibit magnetic order, a parent gapless quantum SL could be lurking in close proximity to these ordered phases. While bond-anisotropic interactions are relevant to some of the observations [46, 52, 55], *ab initio* and exact diagonalization (ED) calculations of the magnetic exchange interactions [56–58], as well as detailed fits to high resolution inelastic neutron scattering data on $BaCo_2(AsO_4)_2$ [41], suggest that a more appropriate starting point is an XXZ ferromagnet, with easy-plane anisotropy, and frustration arising from third-neighbor antiferromagnetic (AFM) exchange. Could such XXZ models in the J_1-J_3 parameter space with subdominant bond-anisotropic exchanges support quantum SLs distinct from the Kitaev SL? If so, can such SLs explain the dynamical THz spin response [40] and the unusual remarkable metallic thermal transport observed in a Mott insulator [42, 48]? Addressing these questions can open up new lines of investigation into these exotic magnetic fluids.

* These authors contributed equally to this work.

The impact of further-neighbor frustration in honeycomb magnets has been previously explored with competing second-neighbor exchange in J_1-J_2 models. For classical Heisenberg models, the ferromagnetic or Néel order of the nearest-neighbor Heisenberg magnet gets destroyed with increasing J_2 [59, 60], leading to coplanar spirals which support a Bose surface of spin wave excitations [61, 62]. In the quantum spin-1/2 Heisenberg antiferromagnet, a regime of this fluctuating spiral order gives way to valence bond crystals [60, 61, 63–66]. In the strong easy-plane limit, this model may realize a gapped (possibly chiral) spin liquid [67–69].

Here, we study the spin-1/2 J_1-J_3 model on the honeycomb lattice, with FM J_1 and frustrating AFM third-neighbor exchange J_3, in the strong easy-plane limit [41, 56, 70], as relevant to the cobaltates, and also explore the impact of weaker bond-dependent exchange couplings. Our main result, obtained using exact diagonalization (ED) and DMRG, is evidence of a distinct intervening phase, between the FM phase at small J_3/J_1 and the zig-zag phase at large J_3/J_1. Given the spin-liquid-like characteristics of this intermediate phase, we label it $\widetilde{\text{SL}}$. Our numerics, however, do not definitively rule out weak symmetry breaking orders in the proposed $\widetilde{\text{SL}}$ state. We present a parton theory and Gutzwiller wavefunction study which suggests that this $\widetilde{\text{SL}}$ state descends from a parent gapless Dirac SL with large low energy spinon density of states. While the Dirac SL state may be ultimately be unstable to $\widetilde{\text{SL}}$ via confinement or spinon pairing, it is nevertheless shown to provide an excellent starting point to describe the experimental THz spin response and thermal conductivity in the honeycomb cobaltates.

I. MODEL HAMILTONIAN

The honeycomb cobaltates have the structure depicted in Fig.1. Their magnetism is described by an easy-plane XXZ spin model, with weaker bond-dependent anisotropies, which was derived using *ab initio* and ED studies [56–58]. In $CoTiO_3$ [50, 51], a dominant FM J_1, with weaker interlayer AFM exchange, leads to in-plane ferromagnetic order staggered from one layer to the next. Small compass anisotropies pin the moment orientation and can induce a weak gap to the Goldstone mode [51, 56]. By contrast, in $BaCo_2(AsO_4)_2$, $BaCo_2(PO_4)_2$, $Na_2Co_2TeO_6$, and $Na_3Co_2SbO_6$, the larger spacing between layers renders the system more two-dimensional (2D), while the pnictogen (P, As, Sb) or chalcogen (Te) mediates significant frustrating antiferromagnetic J_3 [56] 1as also deduced from fits to the neutron scattering data [41]. Motivated by this, we consider the 2D honeycomb lattice XXZ model, with the Hamiltonian

$$\mathcal{H}_1 = \frac{1}{2}\sum_{i,j} J_{ij}\left(S_i^x S_j^x + S_i^y S_j^y + \lambda S_i^z S_j^z\right), \qquad (1)$$

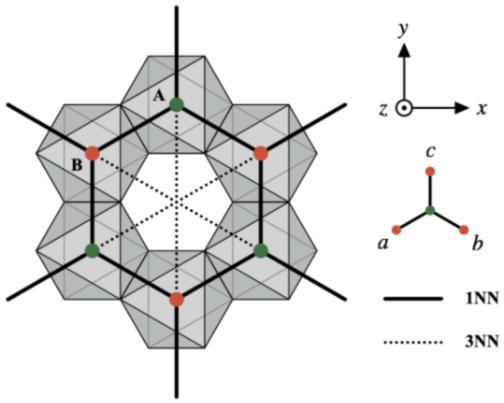

FIG. 1. Schematic view of honeycomb lattice showing pseudospin-1/2 Co^{2+} ions enclosed in edge-sharing oxygen octahedra. Solid lines connecting A-B sublattices represent first-nearest neighbors (1NN), while dotted lines represent third-nearest neighbors (3NN); bonds are labelled (a, b, c) as shown on the right. We also show crystallographic xyz coordinate system which is used for the Hamiltonian.

written in the global xyz basis, where $\hat{z}$ is perpendicular to the honeycomb plane as shown in Fig.1. The exchange couplings J_{ij} are chosen to be ferromagnetic $J_{ij} = -J_1$ for the first neighbor bond, and frustrating antiferromagnetic $J_{ij} = +J_3$ for the third neighbor bond, with $J_1, J_3 > 0$. The Heisenberg limit of this model, $\lambda = 1$, has been partially explored earlier [59, 60] inspired by old experiments on $BaCo_2(AsO_4)_2$ [37]. Here, we focus on the easy-plane regime of interest $0 < \lambda \ll 1$. We supplement this Hamiltonian with weaker nearest-neighbor compass anisotropy terms

$$\mathcal{H}_2 = \sum_{\langle i,j\rangle} \left[\left(K_1\cos\phi_{ij} + K_2\sin\phi_{ij}\right)\left(S_i^x S_j^x - S_i^y S_j^y\right) - \left(K_1\sin\phi_{ij} - K_2\cos\phi_{ij}\right)\left(S_i^x S_j^y + S_i^y S_j^x\right)\right]. \qquad (2)$$

The compass terms have couplings K_1, K_2, with the angles $\phi_{ij} = 0, 2\pi/3, 4\pi/3$ corresponding respectively to the three nearest-neighbor honeycomb bonds c, a, b centered on the A-sublattice (see Fig.1). Motivated by *ab initio* studies [56] and fitting to neutron data [41], we set $K_1 = -K_2 = K$, with $K > 0$ and work in the regime $K \ll J_1$ as relevant to the cobaltates. The total Hamiltonian we study is thus $\mathcal{H} = \mathcal{H}_1 + \mathcal{H}_2$.

II. EXACT DIAGONALIZATION STUDY

We have carried out extensive ED calculations on this model for system sizes ranging from $N = 18$ to $N = 30$ spins (using the Davidson algorithm [71–73]). Fig. 2(a) shows the zero field phase diagram of this model as we vary J_3/J_1 and K/J_1 for fixed $\lambda = 0.25$. Based on studying spin correlations we find (i) an easy-plane FM

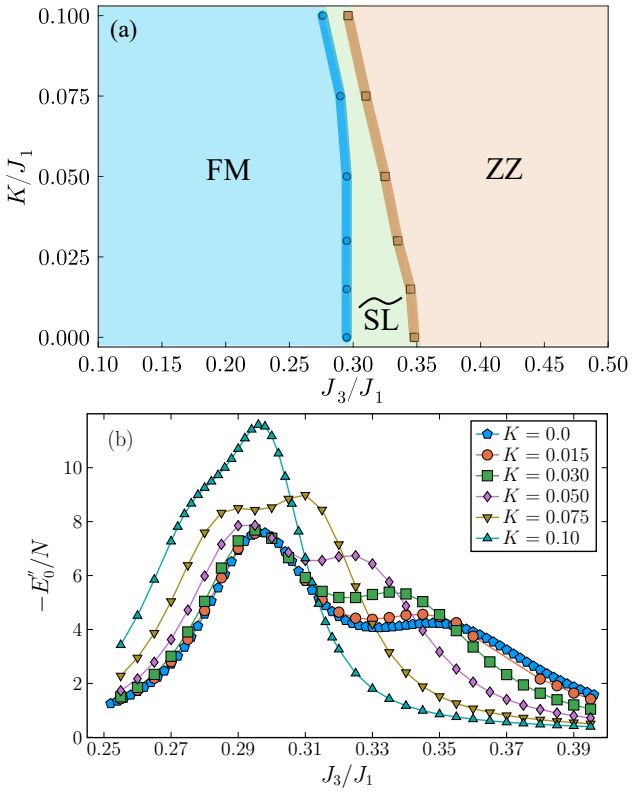

FIG. 2. (a) Phase diagram of the model Hamiltonian $\mathcal{H}$ (see text) for fixed $\lambda = 0.25$ as a function of third-neighbor exchange J_3/J_1 and compass anisotropy K/J_1. Based on ED and DMRG spin correlations, we identify three phases: an easy-plane ferromagnet FM, spin-liquid-like phase $\widetilde{\text{SL}}$, and a zig-zag phase ZZ. The phase boundaries are identified by peaks in ED of $(-\partial^2 E/\partial J_3^2)$. (b) Cuts through the phase diagram in showing $-E_0''/N = (1/N)(-\partial^2 E/\partial J_3^2)$ computed using ED on 24-site torus, as a function of J_3/J_1 for various compass anisotropies K/J_1. The two peaks in $-E_0''/N$ serve to delineate the FM-$\widetilde{\text{SL}}$ and $\widetilde{\text{SL}}$-ZZ phase boundaries.

state for small J_3/J_1, (ii) a zig-zag phase ZZ for large J_3/J_1, and (iii) a small window of an intervening phase where spin correlations appear to exhibit liquid-like behavior [74]; we characterize this phase further below using DMRG calculations on larger system sizes. This intermediate state could arise from quantum disordering the incommensurate spiral order of the classical spin model [60]. Due to the spin-liquid-like nature of this intermediate phase, we term it as $\widetilde{\text{SL}}$. The phase boundaries in Fig. 2(a) are obtained from peaks in the second derivative of the ground state energy with respect to J_3, as shown in in Fig.2(b). With increasing compass anisotropy, the FM-$\widetilde{\text{SL}}$ and $\widetilde{\text{SL}}$-ZZ phase boundaries shift such that the ZZ phase expands as seen from Fig. 2(a) while the FM and $\widetilde{\text{SL}}$ phases shrink. Nevertheless, the intermediate $\widetilde{\text{SL}}$ persists over a window of K/J_1 in this extended phase diagram.

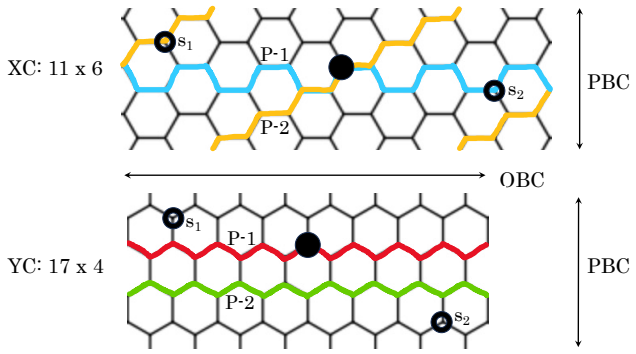

FIG. 3. Cylinder clusters XC (top) and YC (bottom) employed in DMRG calculations with indicated maximum system sizes. We use periodic boundary conditions (PBC) along y and open boundary conditions (OBC) along x. The spin correlations are computed with respect to the reference site (black filled circle) along two indicated paths for each cluster (XC path P-1, blue; XC path P-2, yellow; YC path P-1, red; YC path P-2, green). For finite size scaling of the order parameters we use the spin correlation of sites s_1 and s_2 (open circles) with respect to reference site.

III. DENSITY MATRIX RENORMALIZATION GROUP RESULTS

To further characterize the phases found in ED, we have used the modified DMRG algorithm [75–78] to calculate the ground state of $\mathcal{H}$ on cylinders, studying system sizes upto 66 sites (XC cylinder) and 68 sites (YC cylinder); the clusters are shown in Fig. 3 (see Supplemental Material [74] for details about the DMRG and for comparison with ED results). We have computed spin correlations, in the three different phases identified in ED, going along different paths as indicated in Fig. 3. These include the labelled zigzag and armchair paths on the honeycomb lattice, with sites indexed by steps n and spin correlations computed with respect to the reference point marked by a filled circle. Since the intermediate $\widetilde{\text{SL}}$ phase identified in ED is most visible at $K = 0$, we focus on the parameter set $K/J_1 = 0$ and $\lambda = 0.25$. In this case, the S^x and S^y correlations are identical but they differ from the S^z correlations.

Fig. 4(a) shows the $S^{x,y}$ correlations on the 66-site XC cluster along path P-1 (blue armchair path in Fig. 3). The spin correlations for $J_3/J_1 = 0.2$ and $J_3/J_1 = 0.5$ respectively indicate FM and period-2 ZZ order, while they decay rapidly in the intermediate $\widetilde{\text{SL}}$ phase. The spin correlations along path P-2 (yellow zigzag path Fig. 3) of the XC-cluster show qualitatively similar results as displayed in Fig. 4(b). By contrast, the S^z correlations decay rapidly to zero in all three phases as seen for both path P-1 and path P-2 as seen from Figs. 4(c) and 4(d). We find no evidence for any tendency to incommensurate correlations or other wavevectors in our study.

Turning to the YC-cluster, we find somewhat ambiguous results. Fig. 5(a) and Fig. 5(c) show that the $S^{x,y}$

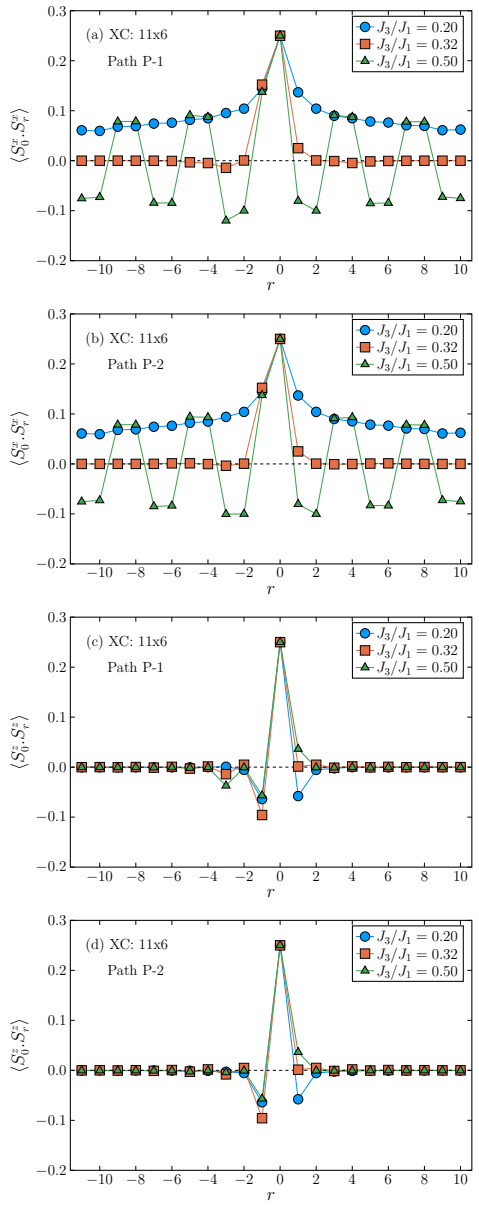

FIG. 4. DMRG spin correlations on XC cluster with respect to the reference site shown in Fig. 3 for $(K = 0, \lambda = 0.25)$. (a) S^x correlations along path P-1 showing FM behavior at $J_3/J_1 = 0.2$, ZZ order at $J_3/J_1 = 0.5$, and spin-liquid-like short range correlations at $J_3/J_1 = 0.32$. (b) Similar to (a) but for path P-2. (c) and (d) S^z correlations showing that they rapidly decay to zero for both paths in all phases.

long ranged spin correlations in the FM and ZZ phases along path P-1 and path P-2 are qualitatively consistent with our findings on the XC-cluster. However, in the intermediate $\widetilde{\text{SL}}$ phase, the $S^{x,y}$ correlations along path P-1 seem to indicate long-range order while it is nearly vanishing along path P-2. This striking spatial anisotropy — relatively long correlations along the same zigzag chain but strongly suppressed correlations with the neighboring zigzag chain — is somewhat reminiscent of sliding Luttinger liquid phases [79–81]. Such sliding phases have also been proposed to occur, on intermediate energy scales, in certain crossed spin-chain models [82, 83]. This spatial anisotropy of correlations observed in the $\widetilde{\text{SL}}$ phase on the YC-cluster might reflect the physics of a strongly fluctuating and partially melted incommensurate spiral order which decouples adjacent zigzag chains. In this YC geometry, the S^z correlations are ambiguous. From Fig. 5(b) and Fig. 5(d), S^z correlations along path-1 are oscillatory, indicative of S^z Néel order (z-Néel) on the honeycomb lattice. However, Fig. 5(d) shows that such oscillatory S^z correlations are also found in the ZZ phase (but not in FM) even for our largest system size, suggesting that these S^z correlations might be strongly influenced by the YC cylinder geometry and are not necessarily a distinguishing feature of $\widetilde{\text{SL}}$.

We have studied the the finite size scaling of S^x, S^y spin correlations on the XC and YC clusters at distant points s_1 and s_2 with respect to the reference site (see Fig. 3). These points are chosen to be one layer away from the boundary to decrease edge effects. We computed these spin correlations extrapolated to the large cylinder size limit as a measure of m^2, the square of the magnetic order parameter. As shown in Fig. 6(a) for the XC cluster, we find nonzero extrapolated FM order at small J_3/J_1 (blue circles, blue squares), and ZZ order at large J_3/J_1 (orange circles and orange squares). This leaves a window $0.3 \lesssim J_3/J_1 \lesssim 0.33$ where such magnetic orders appear to vanish as indicated by the open symbols. For the YC cluster, we find similar results as seen in Fig. 6(b); although the extrapolated correlation for site s_1 suggests a very narrow intermediate phase or a direct transition, there is a clear intermediate phase from studying correlations for site s_2.

We have checked that, together with no clear evidence of magnetic orders, there is also no evidence of Kekulé type valence bond orders in the intermediate window with no FM and ZZ order. Our results are thus strongly suggestive of an intermediate SL phase, distinct from the FM and ZZ phases. Nevertheless, given the ambiguity in our DMRG spin correlation results between the XC and YC clusters, we continue to label this phase as $\widetilde{\text{SL}}$ to highlight its spin-liquid-like character.

We emphasize that our results do not definitively rule out weak broken symmetries in the $\widetilde{\text{SL}}$ phase which might become apparent on larger system sizes. Indeed, after the initial report of our work [84], a more recent DMRG study of this model by Jiang, White, and Chernyshev [85], has reported evidence for an intervening phase consistent with our results. However, they conclude from studying larger cylinder system sizes that this intermediate phase, which we call $\widetilde{\text{SL}}$, is a symmetry broken phase with weak z-Néel order. Crucially, they deduce this order using finite-size scaling of the induced order in the presence of an additional strong z-Néel boundary pinning field. Whether our results differ from their work due to this difference in methodology, or simply due to

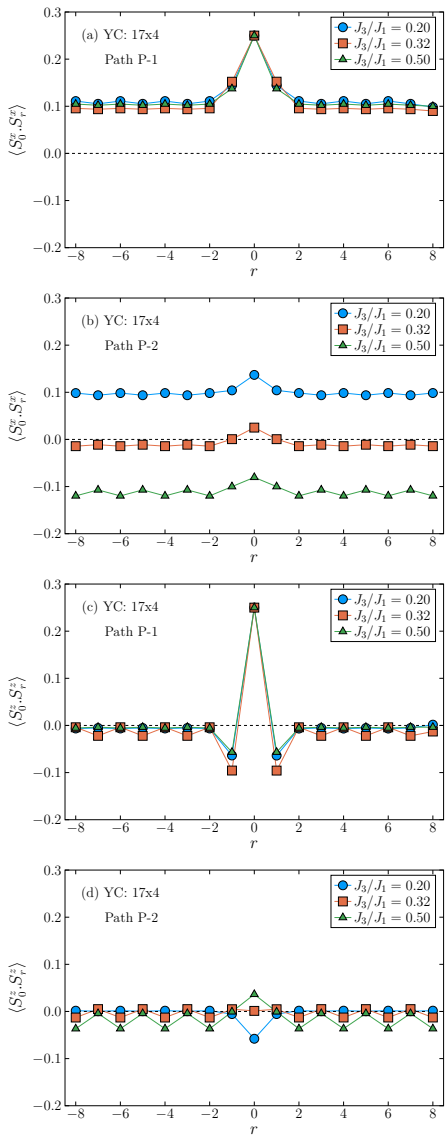

FIG. 5. DMRG spin correlations on YC cluster computed for $(K = 0, \lambda = 0.25)$. (a) S^x correlations along path P-1 showing apparently non-decaying correlations in all phases. (b) S^x correlations along path P-2 showing FM, ZZ, and strongly suppressed correlations for indicated J_3/J_1 values. (c) and (d) show S^z correlations which exhibit weak oscillatory component indicative of z-Néel order for $J_3/J_1 = 0.32$ in the $\widetilde{\text{SL}}$ phase, but these oscillations are more pronounced in the ZZ phase for path P-2 on this YC cluster.

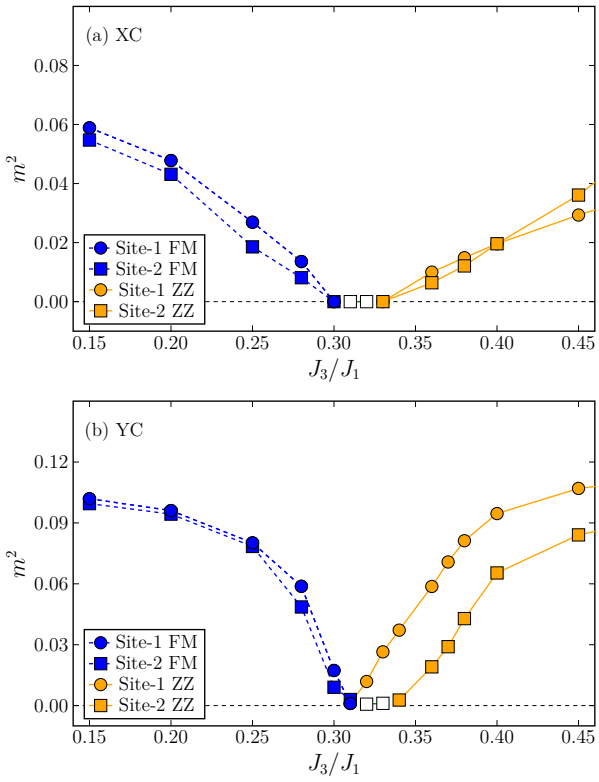

FIG. 6. Extrapolated $\langle S^x_0 S^x_r \rangle$ correlations at distant points s_1 and s_2 with respect to the reference site in the limit of large cylinder sizes for $(K = 0, \lambda = 0.25)$. The dashed (FM) and solid (ZZ) lines are a guide to the eye. (a) XC cluster and (b) YC cluster. These extrapolated correlations indicate an intermediate phase (open squares) which is neither FM nor ZZ. This window is similar in three of the four cases, $0.3 \lesssim J_3/J_1 \lesssim 0.33$, except the result from extrapolating the s_1 correlation in the YC cluster which shows either a very narrow $\widetilde{\text{SL}}$ window or even a direct FM-ZZ transition. We denote this extrapolated correlation as m^2 since it is expected to be a measure of the square of the order parameter (for the FM or ZZ orders). Open squares correspond to nearly vanishing m^2 which is the $\widetilde{\text{SL}}$ phase.

a difference in system sizes, remains to be clarified. We leave this as an open issue for further studies. Moreover, even if we take into account the larger system DMRG results which argue that this $\widetilde{\text{SL}}$ state hosts z-Néel order, the deduced order parameter they deduce is very small, $\lesssim 0.1$, suggesting extremely strong quantum fluctuations in this $\widetilde{\text{SL}}$ state. This places it in proximity to a genuine SL state and well beyond the purview of any linear spin-wave theory description. A pseudo-fermion functional renormalization group study (pf-FRG) of this model [86] has also found a small intervening state with z-Néel order, but the quantitative reliability of this method for identifying phases of spin-1/2 models is unclear.

To conclude this section, our DMRG results for the spin-1/2 J_1-J_3 XXZ model on the honeycomb lattice finds evidence for the $\widetilde{\text{SL}}$ phase, with spin-liquid-like characteristics, at intermediate J_3/J_1. Whether or not the $\widetilde{\text{SL}}$ hosts weak symmetry breaking (e.g., weak z-Néel order), it is important to understand the nature of the proximate SL state from which this phase descends, and to explore its implications for the phase diagram and for experiments on the honeycomb cobaltates. We next turn to this issue using parton mean field theory and a numerical variational Monte Carlo study of Gutzwiller projected parton wavefunctions.

IV. GUTZWILLER PROJECTED PARTON WAVEFUNCTIONS

To identify a candidate for the $\widetilde{\text{SL}}$ phase, we turn to a parton theory of the spin Hamiltonian, using Schwinger fermions to represent spins via $S_i^\mu = \frac{1}{2} f_{i\gamma}^\dagger \sigma_{\gamma\delta}^\mu f_{i\delta}$, where σ^μ are the Pauli matrices. The spin Hamiltonian $\mathcal{H}$ is then expressed as a quartic interaction in terms of partons, and we have to impose $\sum_\gamma f_{i\gamma}^\dagger f_{i\gamma} = 1$ as a local Hilbert space constraint to faithfully represent spin configurations.

A. Parton mean field theory

We can simplify $\mathcal{H}$ expressed in terms of partons using mean field theory where we allow nonzero expectation values for parton bilinears in multiple channels: the Weiss channel which permits magnetic order $\langle S_i^a \rangle \neq 0$ and the hopping channel $\langle f_{i\gamma}^\dagger f_{j\delta} \rangle \equiv W_{ij}^{\gamma\delta}$ which allows parton dispersion. Since mean field theory overestimates the tendency to order, we propose a modified parton mean field theory, replacing

$$\left\langle S_i^\mu S_j^\nu \right\rangle = (1-\alpha) \left\langle S_i^\mu \right\rangle \left\langle S_j^\nu \right\rangle - \frac{1}{4} \mathrm{Tr}\left(\sigma^\mu W_{ij}^* \sigma^\nu W_{ij}^T\right) \quad (3)$$

while computing the mean field energy; this rescales the Weiss channel energy by $(1-\alpha)$. When $\alpha = 0$, we find that the mean field solution converges to the classical magnetically ordered phases with no spinon hopping ($W_{ij} = 0$), reproducing the classical phase diagram of the J_1-J_3 XY model. The choice of intermediate values $0 < \alpha < 1$ phenomenologically incorporates quantum fluctuation effects beyond parton mean field theory. For $\alpha = 1$, magnetic orders are completely suppressed by hand and we find pure spin liquid solutions.

For $\alpha = 1$, we have done the parton mean field theory calculations, exploring possible spatially inhomogeneous solutions directly in real space mean field theory, as well as using momentum space mean field theory with various unit cell sizes. Motivated by the THz [40] and thermal conductivity [48] experiments which find an abundance of low energy excitations, we have chosen to restrict our attention to spin liquids without spinon pairing terms (which might potentially open gaps in the excitation spectrum). In all cases examined, we find that the mean field theory converges to a SL phase which corresponds to a zero flux-state, described by the spinon Hamiltonian $\mathcal{H}_{\text{sp}} = -\sum_{i,j} t_{ij}^{\mu\nu} f_{i,\mu}^\dagger f_{j,\nu}$ with μ, ν denoting spin. Here, the nearest-neighbor parton hopping matrix is $t_{ij} = \sigma_z t_1$ and third-neighbor hopping is $t_{ij} = \sigma_z t_3$ with $t_1, t_3 > 0$, such that the $\uparrow$ and $\downarrow$ spinons each see zero flux on all plaquettes on the honeycomb lattice, but have opposite sign hopping amplitudes relative to each other. This breaks the global $SU(2)$ spin rotation symmetry down to a $U(1)$ spin rotation symmetry, consistent with a wavefunction for an XXZ model. The mean field parton band dispersion with t_1, t_3 hoppings is particle-hole symmetric, with $t_1 \approx 0.13 J_1$ and $t_3/t_1 \approx 0.15$, and features Dirac nodes at the K, K' points of the hexagonal Brillouin zone (BZ) as shown in Fig. 7, so this state is a Dirac SL. We note that a similar Dirac SL, but with first and second neighbor hopping, also appears as a proximate state in the J_1-J_2 honeycomb XY model [68] although its physical properties and relevance to magnetic solids have not been explored.

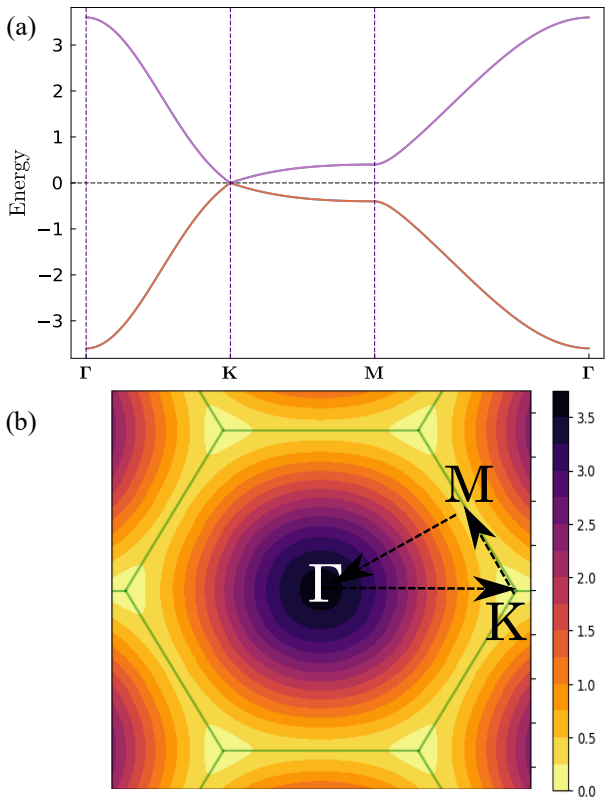

FIG. 7. (a) Mean field parton band structure of the Dirac SL in the original BZ along a path through the Γ-K-M points. Energy is measured in units of t_1, and we have set $t_3/t_1 = 0.2$ as found from our VMC optimization. In self-consistent parton mean field theory, we find a slightly smaller value $t_3/t_1 = 0.15$. (b) Energy gap in units of t_1, shown using color scale, in the full hexagonal BZ - we find low energy modes along the entire edge of the BZ with vanishing gap at the Dirac K points.

B. Variational Monte Carlo study

Going beyond mean field theory, we have studied the phase diagram of the J_1-J_3 XXZ model using Gutzwiller projected parton wavefunctions. We compute the energy and correlations of the projected wavefunction through a Monte Carlo sampling of real space configurations which obey the strict Hilbert space constraint. To obtain the best variational ground state with the lowest energy, and

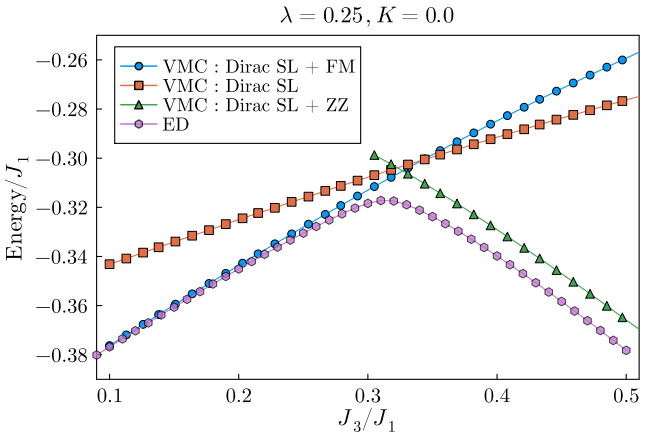

FIG. 8. VMC optimized energies on $N = 24$ sites cluster as a function of J_3/J_1, for different ansatzes, compared with ED energies on the same cluster. We have fixed $\lambda = 0.25$ and $K = 0$. In the FM phase, the VMC energy is within 0.1-0.5% of the ED. In the ZZ phase VMC is within 2-3% of ED. The largest difference of $\approx 4\%$ occurs for $J_3/J_1 \approx 0.32$ where the VMC energy of the Dirac SL is comparable to that of the Dirac SL with coexisting FM or ZZ order.

to study its correlations, we first optimize the variational parameters encoded in the parton mean field Hamiltonian. In our variational wavefunction, we fix $t_1 = 1$ in the parton Hamiltonian, and treat t_3, the on-site Weiss fields B_i (which allow for FM, ZZ, or z-Néel order), and long-range Jastrow factors as variational parameters. For optimizing these parameters, we use the state of the art stochastic reconfiguration technique (a modified gradient descent method) [87].

We focus below on VMC results for the 24-site cluster which we compare with our ED results in Table I; this allows independent Jastrow factors upto third-nearest neighbors. We worked with 10,000 thermalization sweeps followed by 10,000 measurement sweeps for *each* Monte Carlo run. We performed 500 such Monte Carlo runs per optimization, checking that the stochastic reconfiguration drives the variational parameters towards the optimum value in between runs.

As seen from Fig. 8 and Table I we find that the optimal state for $J_3/J_1 \lesssim 0.3$ corresponds to a Dirac SL state with imposed FM order - its energy matches with the ED energies extremely well (we label this state 'SL + FM'). For $J_3/J_1 \gtrsim 0.33$, the optimal state is a Dirac SL state with imposed ZZ order - this exhibits a good energy match to within 2-3% of the ED result (we label this state 'Dirac SL + ZZ') In the intermediate regime, $0.3 \lesssim J_3/J_1 \lesssim 0.33$, we find all ansatzes (Dirac SL, Dirac SL+FM, and Dirac SL+ZZ) to be very close to each other, with the largest discrepancy with the ED energies being $\sim 4\%$. These energy differences between ED and VMC are comparable to the previous best VMC results on the J_1-J_2 honeycomb XY model [67, 68]. The Gutzwiller projected Dirac SL parton state thus captures a large fraction $\sim 96\%$ of the ED energy in the $\widetilde{\text{SL}}$ regime. The Gutzwiller projected Dirac SL has rapidly decaying S^z correlations, while the XY spin correlations decay as $\sim 1/r^\alpha$, with $\alpha \approx 1.5$.

J_3/J_1	E.D.	Dirac SL+FM	Dirac SL	Dirac SL+ZZ
0.24	-0.33331	-0.33114(4)	-0.31797(4)	-0.31806(4)
0.28	-0.32265	-0.31897(4)	-0.31110(4)	-0.31122(4)
0.32	-0.31743	-0.30721(4)	-0.30441(4)	-0.30302(4)
0.36	-0.32266	-0.29581(4)	-0.29790(4)	-0.31555(4)
0.40	-0.33978	-0.28481(4)	-0.29148(4)	-0.32908(4)

TABLE I. Optimized VMC ground state energies (per spin) for the three ansatzes, as compared to the results from exact diagonalization on the 24-site cluster.

C. Relation between $\widetilde{\text{SL}}$ and the Dirac SL: Deformations of Dirac SL

As described in the previous section, the Gutzwiller projected Dirac SL captures 96% of the ED energy for $0.3 \lesssim J_3/J_1 \lesssim 0.32$. This suggests that we can treat the Dirac SL as a proximate parent SL state (i.e., a SL very close by in energy), and the $\widetilde{\text{SL}}$ state observed in this window (in ED and DMRG) as a related descendant. In field theory language, the Dirac SL we have found involves $N_f = 4$ flavors of massless two-component Dirac fermions coupled to an $SU(2)$ gauge field. Large-N_f versions of closely related theories have been studied in previous work [88–91]; however, the low energy fate of this theory is unclear at $N_f = 4$. In this framework, the $\widetilde{\text{SL}}$ phase might descend from the Dirac SL as a result of symmetry breaking or spinon pairing or confinement. To explore this in VMC, we have incorporated various mass terms in our Dirac SL ansatz, as well as rotational symmetry breaking hoppings (nematic order).

We find that Dirac mass terms such as the (i) time-reversal preserving Kane-Mele (quantum spin Hall) mass, (ii) the time-reversal breaking Haldane (chiral) mass, or (iii) a Kekulé mass which leads to $\sqrt{3} \times \sqrt{3}$ valence bond order, do not lower the energy of the Dirac SL. Motivated by related DMRG work [85] and pf-FRG results [86], we have also considered (iv) a z-Néel mass, but also do not find it to be favored within VMC. We found that a rotational symmetry breaking nearest-neighbour hopping decreased the energy, but only in the ZZ phase and by a negligibly small value $\approx 0.1\%$; this is too small to impact our comparison with ED. Given the computational complexity of studying spinon pairing states in XXZ models within VMC (which must account for coexisting singlet and triplet pairing), we defer a study of such pairing states, as well an exhaustive study for all Dirac mass terms, to a future investigation.

In order to examine how some of these perturbations, specifically the FM, ZZ, and z-Néel order, impact the

mean field parton dispersion, we studied the effect of such perturbations on the single-particle band structure. As seen from Fig. 9(a), including a z-Néel Weiss field in the Dirac SL parton ansatz gaps out the Dirac touchings at the K points. Fig. 9(b) shows that an in-plane FM Weiss field, which is equivalent to an in-plane Zeeman field, has a very similar effect. This is an interesting point to keep in mind when later examine experimentally relevant response functions of the Dirac SL. In particular, although $\widetilde{\text{SL}}$ might be a weakly gapped/ordered phase descending from the Dirac SL, its high energy response in all these cases will look very similar to the Dirac SL. Moreover, weak disorder-induced broadening of the parton spectral functions on the scale of a small Dirac mass gap might lead to apparent gapless behavior even at low energy.

Unlike the FM and z-Néel order, the ZZ Weiss field is not a simple Dirac mass term . Here, we work with the quadrupled 2×2 unit cell (8 site unit cell) which accommodates the ZZ ordering. With increasing m_{ZZ}, the Dirac points persist as gapless band touching points (although they can shift in momentum), so this parton mean field state would have ZZ order coexisting with fractionalized gapless excitations. Such a state has been conjectured to occur in $Na_2Co_2TeO_6$ [48]. Fig. 9(c) shows that for $m_{ZZ} \approx 0.1$ there is a band touching at the Γ_R point of the folded BZ. Further increase of m_{ZZ} leads to a quadratic band touching at M_{2R} for $m_{ZZ} \approx 0.25$, before the bands eventually get fully gapped out for $m_{ZZ} \gtrsim 0.25$.

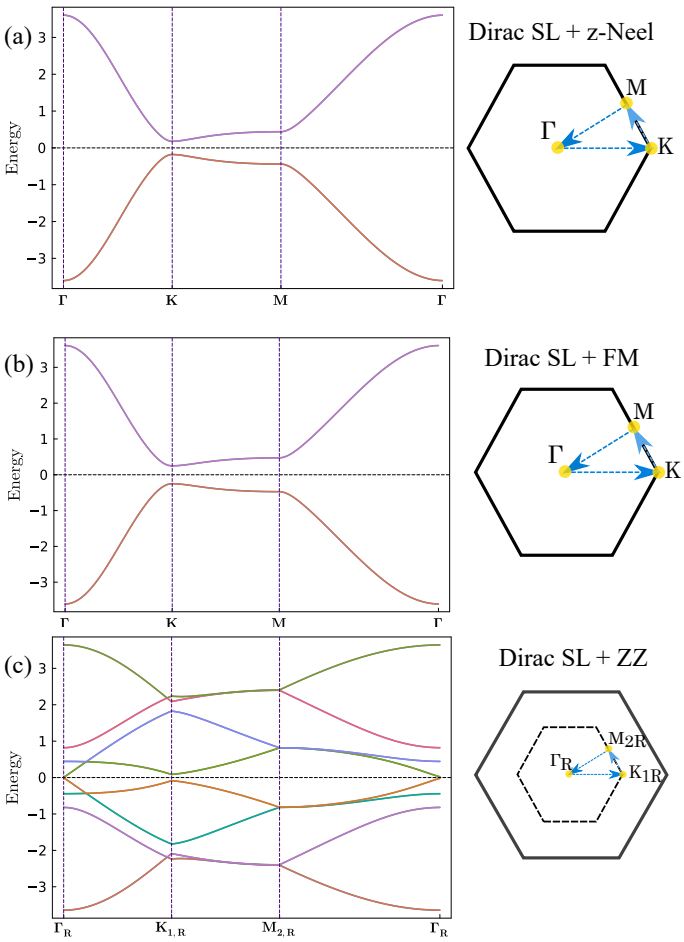

FIG. 9. Mean field parton band structures of the perturbed Dirac SL (with energy in units of t_1) for $t_3/t_1 = 0.2$. (a) Band structure in the original BZ with z-Néel order parameter $m^z_{\text{N}} = 0.1$ showing that the Dirac nodes get gapped out. (b) Band structure with in-plane Zeeman field $h/t_1 = 0.5$ showing that the Dirac nodes get gapped out. (c) Band structure in the reduced BZ (dashed line) for 2×2 unit cell in the presence of ZZ order with order parameter $m_{\text{ZZ}} = 0.1$ showing that band touching points persist (here at Γ_R). The ZZ order is chosen with wavevector $(0, \pi)$. For large $m_{\text{ZZ}} \gtrsim 0.25$, the dispersion is fully gapped at the chemical potential ($E = 0$).

V. EXPERIMENTAL IMPLICATIONS

With the above results on the phase diagram and the variational wavefunction in hand, we next turn to a discussion of the experimental data on the honeycomb cobaltates which exhibit SL like characteristics such as a broad continuum in THz spectroscopy and a low temperature metallic thermal conductivity. The ideal comparison between theory and experiments would have been to explore response and transport in the $\widetilde{\text{SL}}$ ground state. However, given our difficulty in identifying the precise nature of the $\widetilde{\text{SL}}$ phase, and the considerable challenge of exploring dynamics and transport in this strongly fluctuating state, we take a slightly simpler tack here and explore the corresponding results in the parent Dirac SL state using parton mean field theory. Remarkably, we find that the Dirac SL, within parton mean field theory, provides an excellent semi-quantitative description of the existing THz and metallic thermal conductivity data in these cobaltates. We speculate that the reason for this good agreement might be that at intermediate energy scales, or in the presence of weak disorder or thermal fluctuations in the real materials, the balance might shift in favor of the parent Dirac SL over the $\widetilde{\text{SL}}$ state as a reasonable description of the spin-liquid-like behavior found in the cobaltates.

A. THz spin dynamics

Using the Dirac SL ansatz, we have calculated the THz spin response in terms of the mean field parton Green functions using the bubble diagram to obtain the spin susceptibility. The zero momentum response is given by

$$\chi_{ab}(i\Omega_n) = -\frac{1}{4}\sum_{\mathbf{k},\,\omega_n} \text{Tr}[\sigma^a G^T(\mathbf{k}, i\omega_n)\sigma^b G^T(\mathbf{k}, i\omega_n + i\Omega_n)] \quad (4)$$

where $G^{\alpha\beta}_{ij}(\mathbf{k}, i\omega_n) = \left\langle f^\dagger_{i\alpha}(\mathbf{k}, i\omega_n) f_{j\beta}(\mathbf{k}, i\omega_n)\right\rangle$. We can analytically continue $\chi_{ab}(i\Omega_n \to \Omega + i0^+)$ to obtain the real frequency response.

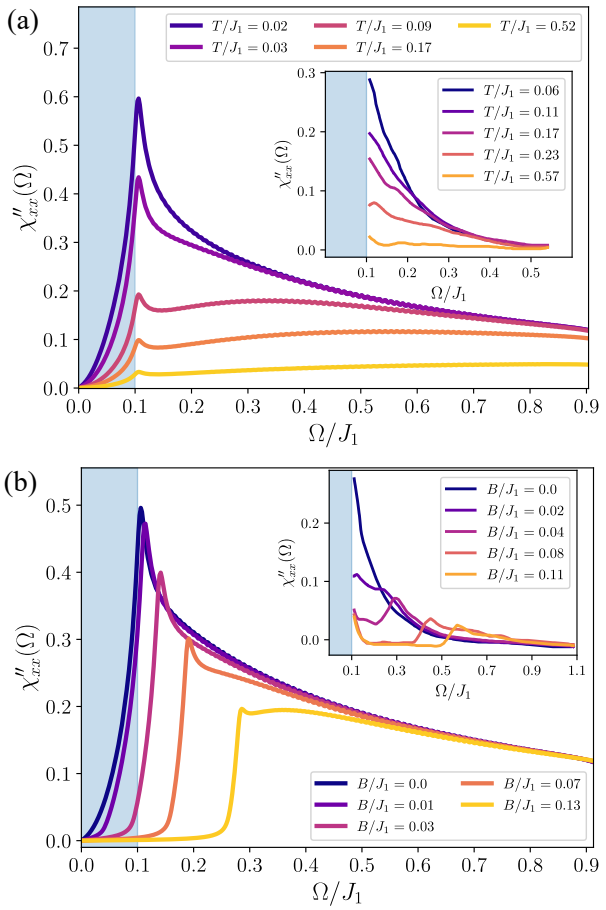

FIG. 10. Imaginary part of the dynamic spin susceptibility od Dirac SL at zero momentum $\chi''_{xx}(\Omega)$, **a.** as a function of varying temperatures T at $B = 0$, and **b.** at a fixed T with varying in-plane B along $\hat{x}$. Insets show corresponding experimental THz spectroscopy data for $BaCo_2(AsO_4)_2$ [40]; we use $B = g\mu_B H$ with $g \approx 5$ and H measured in Tesla, and $J_1 = 7.6\,\text{meV}$ to scale the experimental data [40, 41]. The shaded regions correspond to frequency windows not explored in the THz measurements.

Fig. 10(a) shows the real frequency zero wavevector THz spin response, the imaginary component $\chi''_{xx}(\Omega)$, plotted at zero field as function of frequency Ω, for various temperatures T, in the mean field Dirac SL with $t_1 = 0.13J_1$ and $t_3/t_1 = 0.2$. As we cool from high T, $\chi''_{xx}(\Omega)$ develops a broad feature which is strongly enhanced as a low frequency 'peak', before decreasing for $\Omega/J_1 \lesssim 0.1$. This enhancement arises from the large low energy density of states for spinon excitations around the entire BZ edge, as seen from Fig. 7, with the peak coming from states at the M point of the original honeycomb BZ. For comparison, the inset of Fig. 10(a) shows the experimental data on $BaCo_2(AsO_4)_2$ [40], which highlights their striking similarity. We note that the THz absorption data on $BaCo_2(AsO_4)_2$ [40] does not extend below $\lesssim 0.2\,\text{THz}$; using $J_1 = 7.6\,\text{meV}$ [41], this corresponds to $\Omega/J_1 \lesssim 0.1$. We mark this frequency cutoff in our theoretical plot Fig. 10**a** and in the experimental data in the inset. Extrapolating the THz data to lower frequency using constraints from Kramers-Krönig relations [40] does seem to suggest that the response decreases below $\lesssim 0.2\,\text{THz}$, which would be consistent with the Dirac SL. We have checked that incorporating a small Dirac mass, for instance via weak z-Néel order, leaves the high energy continuum unaffected while inducing a small gap at very low energies, so this would still be consistent with the experimental THz data.

Fig. 10(b) shows that an in-plane Zeeman field digs out a low energy spectral gap which increases with the field, while the high frequency response remains broad. This gap is because the in-plane field induces the mixing and splitting of degenerate spin-↑ and spin-↓ parton bands. We have set $B = g\mu_B H$ for the in-plane field, with $g = 5$ [40, 56] and H measured in Tesla. This behavior is also qualitatively similar to the experimental data on $BaCo_2(AsO_4)_2$ [40], which is replotted in the inset, although the theoretical gap scale is smaller by a factor of ~ 2 for comparable B/J_1. We attribute this difference to parton mean field theory underestimating the internal Zeeman field generated by J_1, which can significantly boost the gap as the uniform magnetization increases.

At high field, the gapped experimental data may be better thought of in terms of gapped spin-1 magnons around a polarized state; in the parton theory, the magnons arise most simply as bound states of the spin-1/2 partons. However, the full theory of this magnon-parton response needs a more careful discussion of confinement effects which deserves a separate investigation.

B. Low temperature thermal conductivity

Within parton mean field theory, the low temperature 2D longitudinal thermal conductivity may be obtained indirectly by assigning a conserved 'electric charge' $e_\star$ to the spinons, computing the bubble diagram for the 2D longitudinal 'electrical conductivity' $\sigma \propto e_\star^2$, and appealing to the Wiedemann-Franz law to extract $\kappa/T = \sigma L$ where the Lorenz number $L = \pi^2 k_B^2/3e_\star^2$; the charge $e_\star$ thus drops out of the final result for κ/T. We obtain σ using the bubble diagram with disorder-broadened Green functions,

$$\text{Re}(\sigma^{\mu\nu}) = -\frac{e_\star^2}{\hbar}\sum_{\mathbf{k}} \text{Tr}\left[v^\mu(\mathbf{k})A(\mathbf{k},0)v^\nu(\mathbf{k})A(\mathbf{k},0)\right] \quad (5)$$

where $v^\mu(\mathbf{k}) = \partial H/\partial \mathbf{k}_\mu$ are velocity matrices, with H being the parton mean field Hamiltonian for the Dirac SL (or Dirac SL with coexisting ZZ or z-Néel order), and $A(\mathbf{k},\omega)$ is the spectral function matrix. The source of this disorder might be, for example, Na positional disorder in $Na_2Co_2TeO_6$ [92]. The inferred κ/T is plotted in Fig. 11(a) as a function of the disorder broadening Γ for the Dirac SL, as well as for the Dirac SL with coexisting FM, or z-Néel, or ZZ order. For com-

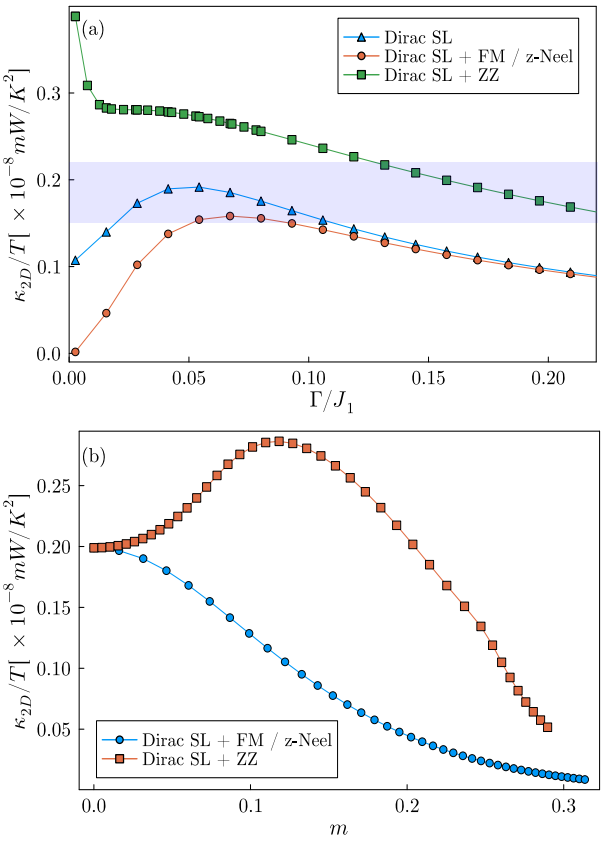

FIG. 11. 2D thermal conductivity $\kappa_{\rm avg}/T = (\kappa_{xx} + \kappa_{yy})/2T$ (in physical units) for the Dirac SL from parton mean field theory with $t_3/t_1 = 0.2$ and weak disorder induced broadening Γ. (a) $\kappa_{\rm avg}/T$ as a function disorder-induced broadening Γ for (i) the Dirac SL, (ii) for Dirac SL with coexisting z-Néel or FM order with fixed order parameter of $m = 0.1$ (both yield almost identical result), and (iii) coexisting ZZ order with fixed order parameter of $m = 0.1$. The purple band indicates the range of experimental values of κ/T in $Na_2Co_2TeO_6$. (b) $\kappa_{\rm avg}$ for Dirac SL with fixed disorder broadening $\Gamma = 0.025J_1$ and coexisting magnetic order (z-Néel/FM or ZZ) with varying order parameter m.

parison, Fig. 11(a) also shows the band of experimentally reported values in $Na_2Co_2TeO_6$ [48] at zero field in the ZZ phase. Here, we have multiplied the measured 3D value of $\kappa/T \approx 0.03$-$0.04\,\mathrm{mW/K^2cm}$ by the honeycomb interlayer spacing $d_c = 5.63$Å for $Na_2Co_2TeO_6$ [93] to get the experimental result for κ/T per 2D honeycomb plane. We find reasonable agreement between experiment and theory (for 'Dirac SL + ZZ') over a wide range of Γ/J_1. Metallic thermal conductivity has also been reported in $BaCo_2(AsO_4)_2$ [42], but only when the magnetic order is suppressed to reveal a window of SL. For $BaCo_2(AsO_4)_2$, $d_c = 7.83$Å and the metallic $\kappa/T \approx 0.03$-$0.06\,\mathrm{mW\ K^{-2}cm^{-1}}$ [42], which leads to the 2D $\kappa/T \approx 0.23$-$0.46 \times 10^{-8}\,\mathrm{mW\ K^{-2}}$ per honeycomb plane, in rough agreement with the theoretical estimate for the Dirac SL (over a range of Γ) in Fig. 11(a).

Fig. 11(b) shows the dependence of κ/T per honeycomb layer on the strength of coexisting FM, or z-Néel, or ZZ order parameter. While the FM and z-Néel orders monotonically suppress the thermal conductivity due to gapping of the Dirac nodes (see Figs. 9(a) and 9(b)), the dependence on the ZZ order parameter is non-monotonic since the Dirac nodes persist, and additional quadratic band touching points appear in the dispersion, before the spinons get fully gapped; cobaltates with more strong ZZ order should thus have a very strongly suppressed κ/T at low temperature.

VI. DISCUSSION

In summary, we have used ED and DMRG calculations to show that the spin-1/2 J_1-J_3 honeycomb lattice XXZ model exhibits easy-plane FM order at small J_3 and ZZ order at large J_3, separated by a phase which exhibits spin-liquid-like spin correlations at intermediate J_3/J_1. This intervening phase persists in the presence of weak compass anisotropy. Using a modified parton mean field theory, supported by a Gutzwiller wavefunction study, we have identified a candidate Dirac SL state which might be a parent of the numerically observed $\widetilde{\rm SL}$. The parent Dirac SL was shown to qualitatively capture the observed temperature and field dependent broad continuum in THz response of $BaCo_2(AsO_4)_2$ [40], as well as a linear-in-T thermal conductivity even in the presence of coexisting weak symmetry breaking orders if we account for disorder induced broadening of the parton spectral function. The presence of low energy excitations along the entire hexagonal BZ edge in the Dirac SL can also allow a variety of magnetic orders to be energetically competitive and to be stabilized by small changes in the exchange couplings. This provides a parton theory perspective on the diversity of magnetic orders observed in the honeycomb cobaltates.

In future studies, it would be important to study the impact of gauge fluctuations on the dynamical spin response and thermal conductivity presented here. In addition, it would be useful to explore how nonlinear spin wave theory and magnon interaction effects [70] might possibly also lead to SL type signatures in the excitation spectra and how they might also provide a description of thermal conductivity experiments. On the experimental front, looking for THz signatures of low energy excitations in $Na_2Co_2TeO_6$ would provide support for the coexistence of ZZ order and Dirac partons. Investigating these connections would lead to a further understanding of the physics observed in these remarkable quantum magnets.

ACKNOWLEDGEMENTS

We thank Federico Becca, Sasha Chernyshev, and Martin Klanjsek for extremely useful discussions. This re-

search was funded by NSERC of Canada (AB, SV, AP), DST India (MR, SS, MK, and TS-D), and a SERB-India Vajra Fellowship VJR/2019/000076 (AP, TS-D). TS-D acknowledges a J.C.Bose National Fellowship (grant no. JCB/2020/000004) for funding. MK acknowledges support from SERB through grant no. CRG/2020/000754. The parton and VMC computations were carried out on the Niagara supercomputer at the SciNet HPC Consortium and the Digital Research Alliance of Canada. AP acknowledges helpful conversations with Ciaran Hickey, Stephan Rachel, Yasir Iqbal, Matthew Fisher, Oleg Starykh, and Cenke Xu during the KITP workshop "A New Spin on Quantum Magnets", supported in part by the National Science Foundation under Grants No. NSF PHY-1748958 and PHY-2309135.

[1] X. G. Wen, *Quantum field theory of many-body systems: from the origin of sound to an origin of light and electrons* (Oxford University Press, Oxford, 2007).
[2] P. A. Lee, Quantum spin liquid: a tale of emergence from frustration, Journal of Physics: Conference Series **529**, 012001 (2014).
[3] L. Savary and L. Balents, Quantum spin liquids: a review, Reports on Progress in Physics **80**, 016502 (2016).
[4] C. Broholm, R. J. Cava, S. A. Kivelson, D. G. Nocera, M. R. Norman, and T. Senthil, Quantum spin liquids, Science **367**, eaay0668 (2020).
[5] J. Knolle and R. Moessner, A field guide to spin liquids, Annual Review of Condensed Matter Physics **10**, 451 (2019).
[6] P. Anderson, Resonating valence bonds: A new kind of insulator?, Materials Research Bulletin **8**, 153 (1973).
[7] R. Moessner and S. L. Sondhi, Resonating valence bond phase in the triangular lattice quantum dimer model, Phys. Rev. Lett. **86**, 1881 (2001).
[8] P. W. Anderson, The resonating valence bond state in La_2CuO_4 and superconductivity, Science **235**, 1196 (1987).
[9] D. S. Rokhsar and S. A. Kivelson, Superconductivity and the quantum hard-core dimer gas, Phys. Rev. Lett. **61**, 2376 (1988).
[10] A. Kitaev, Anyons in an exactly solved model and beyond, Annals of Physics **321**, 2 (2006).
[11] J. S. Helton, K. Matan, M. P. Shores, E. A. Nytko, B. M. Bartlett, Y. Yoshida, Y. Takano, A. Suslov, Y. Qiu, J.-H. Chung, D. G. Nocera, and Y. S. Lee, Spin dynamics of the spin-1/2 kagome lattice antiferromagnet $ZnCu_3(OH)_6Cl_2$, Phys. Rev. Lett. **98**, 107204 (2007).
[12] P. Mendels and F. Bert, Quantum kagome frustrated antiferromagnets: One route to quantum spin liquids, Comptes Rendus Physique **17**, 455 (2016).
[13] Y. Ran, M. Hermele, P. A. Lee, and X.-G. Wen, Projected-wave-function study of the spin-1/2 Heisenberg model on the kagomé lattice, Phys. Rev. Lett. **98**, 117205 (2007).
[14] Y. Iqbal, F. Becca, S. Sorella, and D. Poilblanc, Gapless spin-liquid phase in the kagome spin-$\frac{1}{2}$ Heisenberg antiferromagnet, Phys. Rev. B **87**, 060405 (2013).
[15] Y.-C. He, M. P. Zaletel, M. Oshikawa, and F. Pollmann, Signatures of Dirac cones in a DMRG study of the kagome Heisenberg model, Phys. Rev. X **7**, 031020 (2017).
[16] Y. Okamoto, M. Nohara, H. Aruga-Katori, and H. Takagi, Spin-liquid state in the $s = 1/2$ hyperkagome antiferromagnet $Na_4Ir_3O_8$, Phys. Rev. Lett. **99**, 137207 (2007).
[17] M. J. Lawler, A. Paramekanti, Y. B. Kim, and L. Balents, Gapless spin liquids on the three-dimensional hyperkagome lattice of $Na_4Ir_3O_8$, Phys. Rev. Lett. **101**, 197202 (2008).
[18] Y. Zhou, P. A. Lee, T.-K. Ng, and F.-C. Zhang, $Na_4Ir_3O_8$ as a 3D spin liquid with fermionic spinons, Phys. Rev. Lett. **101**, 197201 (2008).
[19] K. A. Ross, L. Savary, B. D. Gaulin, and L. Balents, Quantum excitations in quantum spin ice, Phys. Rev. X **1**, 021002 (2011).
[20] M. J. P. Gingras and P. A. McClarty, Quantum spin ice: a search for gapless quantum spin liquids in pyrochlore magnets, Reports on Progress in Physics **77**, 056501 (2014).
[21] Y.-P. Huang, G. Chen, and M. Hermele, Quantum spin ices and topological phases from dipolar-octupolar doublets on the pyrochlore lattice, Phys. Rev. Lett. **112**, 167203 (2014).
[22] R. Sibille, N. Gauthier, H. Yan, M. Ciomaga Hatnean, J. Ollivier, B. Winn, U. Filges, G. Balakrishnan, M. Kenzelmann, N. Shannon, and T. Fennell, Experimental signatures of emergent quantum electrodynamics in $Pr_2Hf_2O_7$, Nature Physics **14**, 711 (2018).
[23] G. Semeghini, H. Levine, A. Keesling, S. Ebadi, T. T. Wang, D. Bluvstein, R. Verresen, H. Pichler, M. Kalinowski, R. Samajdar, A. Omran, S. Sachdev, A. Vishwanath, M. Greiner, V. Vuletic, and M. D. Lukin, Probing topological spin liquids on a programmable quantum simulator, Science **374**, 1242 (2021).
[24] M. Hermanns, I. Kimchi, and J. Knolle, Physics of the Kitaev model: Fractionalization, dynamic correlations, and material connections, Annual Review of Condensed Matter Physics **9**, 17 (2018).
[25] Y. Motome and J. Nasu, Hunting Majorana fermions in Kitaev magnets, Journal of the Physical Society of Japan **89**, 012002 (2020).
[26] G. Jackeli and G. Khaliullin, Mott insulators in the strong spin-orbit coupling limit: From Heisenberg to a quantum compass and Kitaev models, Phys. Rev. Lett. **102**, 017205 (2009).
[27] I. Kimchi and A. Vishwanath, Kitaev-Heisenberg models for iridates on the triangular, hyperkagome, kagome, fcc, and pyrochlore lattices, Phys. Rev. B **89**, 014414 (2014).
[28] H. Takagi, T. Takayama, G. Jackeli, G. Khaliullin, and S. E. Nagler, Concept and realization of Kitaev quantum spin liquids, Nature Reviews Physics **1**, 264 (2019).
[29] S. Trebst and C. Hickey, Kitaev materials, Physics Reports **950**, 1 (2022).
[30] K. W. Plumb, J. P. Clancy, L. J. Sandilands, V. V. Shankar, Y. F. Hu, K. S. Burch, H.-Y. Kee, and Y.-J. Kim, α-$RuCl_3$: A spin-orbit assisted Mott insulator on a honeycomb lattice, Phys. Rev. B **90**, 041112 (2014).

[31] L. J. Sandilands, Y. Tian, K. W. Plumb, Y.-J. Kim, and K. S. Burch, Scattering continuum and possible fractionalized excitations in α-$RuCl_3$, Phys. Rev. Lett. **114**, 147201 (2015).

[32] A. Banerjee, J. Yan, J. Knolle, C. A. Bridges, M. B. Stone, M. D. Lumsden, D. G. Mandrus, D. A. Tennant, R. Moessner, and S. E. Nagler, Neutron scattering in the proximate quantum spin liquid α-$RuCl_3$, Science **356**, 1055 (2017).

[33] G. Baskaran, D. Sen, and R. Shankar, Spin-S Kitaev model: Classical ground states, order from disorder, and exact correlation functions, Phys. Rev. B **78**, 115116 (2008).

[34] P. P. Stavropoulos, D. Pereira, and H.-Y. Kee, Microscopic mechanism for a higher-spin Kitaev model, Phys. Rev. Lett. **123**, 037203 (2019).

[35] H. Liu and G. Khaliullin, Pseudospin exchange interactions in d^7 cobalt compounds: Possible realization of the Kitaev model, Phys. Rev. B **97**, 014407 (2018).

[36] H. Liu, J. c. v. Chaloupka, and G. Khaliullin, Kitaev spin liquid in 3d transition metal compounds, Phys. Rev. Lett. **125**, 047201 (2020).

[37] L. Regnault, P. Burlet, and J. Rossat-Mignod, Magnetic ordering in a planar XY model: $BaCo_2(AsO_4)_2$, Physica B+C **86-88**, 660 (1977).

[38] L. P. Regnault, C. Boullier, and J. E. Lorenzo, Polarized-neutron investigation of magnetic ordering and spin dynamics in $BaCo_2(AsO_4)_2$ frustrated honeycomb-lattice magnet, Heliyon **4**, E00507 (2018).

[39] R. Zhong, T. Gao, N. P. Ong, and R. J. Cava, Weak-field induced nonmagnetic state in a Co-based honeycomb, Science Advances **6 (4)**, aay6953 (2019).

[40] X. Zhang, Y. Xu, T. Halloran, R. Zhong, C. Broholm, R. J. Cava, N. Drichko, and N. P. Armitage, A magnetic continuum in the cobalt-based honeycomb magnet $BaCo_2(AsO_4)_2$, Nature Materials **22**, 58 (2023).

[41] T. Halloran, F. Desrochers, E. Z. Zhang, T. Chen, L. E. Chern, Z. Xu, B. Winn, M. Graves-Brook, M. B. Stone, A. I. Kolesnikov, Y. Qiu, R. Zhong, R. Cava, Y. B. Kim, and C. Broholm, Geometrical frustration versus Kitaev interactions in $BaCo_2(AsO_4)_2$, Proceedings of the National Academy of Sciences **120**, e2215509119 (2023).

[42] C. Tu, D. Dai, X. Zhang, C. Zhao, X. Jin, B. Gao, P. Dai, and S. Li, Evidence for gapless quantum spin liquid in a honeycomb lattice, arXiv e-prints , arXiv:2212.07322 (2022), arXiv:2212.07322 [cond-mat.str-el].

[43] H. S. Nair, J. M. Brown, E. Coldren, G. Hester, M. P. Gelfand, A. Podlesnyak, Q. Huang, and K. A. Ross, Short-range order in the quantum XXZ honeycomb lattice material $BaCo_2(PO_4)_2$, Phys. Rev. B **97**, 134409 (2018).

[44] E. Lefrancois, M. Songvilay, J. Robert, G. Nataf, E. Jordan, L. Chaix, C. V. Colin, P. Lejay, A. Hadj-Azzem, R. Ballou, and V. Simonet, Magnetic properties of the honeycomb oxide $Na_3Co_2TeO_6$, Phys. Rev. B **94**, 214416 (2016).

[45] M. Songvilay, J. Robert, S. Petit, J. A. Rodriguez-Rivera, W. D. Ratcliff, F. Damay, V. Balédent, M. Jiménez-Ruiz, P. Lejay, E. Pachoud, A. Hadj-Azzem, V. Simonet, and C. Stock, Kitaev interactions in the Co honeycomb antiferromagnets $Na_3Co_2SbO_6$ and $Na_3Co_2TeO_6$, Phys. Rev. B **102**, 224429 (2020).

[46] H. Yang, C. Kim, Y. Choi, J. H. Lee, G. Lin, J. Ma, M. Kratochvílová, P. Proschek, E.-G. Moon, K. H. Lee, Y. S. Oh, and J.-G. Park, Significant thermal Hall effect in the 3d cobalt Kitaev system $Na_2Co_2TeO_6$, Phys. Rev. B **106**, L081116 (2022).

[47] S. Zhang, S. Lee, A. J. Woods, S. M. Thomas, R. Movshovich, E. Brosha, Q. Huang, H. Zhou, V. S. Zapf, and M. Lee, Electronic and magnetic phase diagrams of Kitaev quantum spin liquid candidate $Na_2Co_2TeO_6$ (2023), arXiv:2212.03849 [cond-mat.str-el].

[48] S. Guang, N. Li, R. L. Luo, Q. Huang, Y. Wang, X. Yue, K. Xia, Q. Li, X. Zhao, G. Chen, H. Zhou, and X. Sun, Thermal transport of fractionalized antiferromagnetic and field-induced states in the Kitaev material $Na_2Co_2TeO_6$, Phys. Rev. B **107**, 184423 (2023).

[49] J.-Q. Yan, S. Okamoto, Y. Wu, Q. Zheng, H. D. Zhou, H. B. Cao, and M. A. McGuire, Magnetic order in single crystals of $Na_3Co_2SbO_6$ with a honeycomb arrangement of $3d^7$ Co^{2+} ions, Phys. Rev. Materials **3**, 074405 (2019).

[50] B. Yuan, I. Khait, G.-J. Shu, F. C. Chou, M. B. Stone, J. P. Clancy, A. Paramekanti, and Y.-J. Kim, Dirac magnons in a honeycomb lattice quantum XY magnet $CoTiO_3$, Phys. Rev. X **10**, 011062 (2020).

[51] M. Elliot, P. A. McClarty, D. Prabhakaran, R. D. Johnson, H. C. Walker, P. Manuel, and R. Coldea, Order-by-disorder from bond-dependent exchange and intensity signature of nodal quasiparticles in a honeycomb cobaltate, Nature Communications **12**, 3936 (2021).

[52] X. Li, Y. Gu, Y. Chen, V. O. Garlea, K. Iida, K. Kamazawa, Y. Li, G. Deng, Q. Xiao, X. Zheng, Z. Ye, Y. Peng, I. A. Zaliznyak, J. M. Tranquada, and Y. Li, Giant magnetic in-plane anisotropy and competing instabilities in $Na_3Co_2SbO_6$, Phys. Rev. X **12**, 041024 (2022).

[53] W. G. F. Krüger, W. Chen, X. Jin, Y. Li, and L. Janssen, Triple-q order in $Na_2Co_2TeO_6$ from proximity to hidden-SU(2)-symmetric point (2022), arXiv:2211.16957 [cond-mat.str-el].

[54] X. Hong, M. Gillig, W. Yao, L. Janssen, V. Kocsis, S. Gass, Y. Li, A. U. B. Wolter, B. BÃ¼chner, and C. Hess, Phonon thermal transport shaped by strong spin-phonon scattering in a Kitaev material $Na_2Co_2TeO_6$ (2023), arXiv:2306.16963 [cond-mat.str-el].

[55] A. L. Sanders, R. A. Mole, J. Liu, A. J. Brown, D. Yu, C. D. Ling, and S. Rachel, Dominant kitaev interactions in the honeycomb materials $Na_3Co_2SbO_6$ and $Na_2Co_2TeO_6$, Phys. Rev. B **106**, 014413 (2022).

[56] S. Das, S. Voleti, T. Saha-Dasgupta, and A. Paramekanti, Xy magnetism, Kitaev exchange, and long-range frustration in the $J_{\rm eff} = \frac{1}{2}$ honeycomb cobaltates, Phys. Rev. B **104**, 134425 (2021).

[57] P. A. Maksimov, A. V. Ushakov, Z. V. Pchelkina, Y. Li, S. M. Winter, and S. V. Streltsov, Ab initio guided minimal model for the "Kitaev" material $BaCo_2(AsO_4)_2$: Importance of direct hopping, third-neighbor exchange, and quantum fluctuations, Phys. Rev. B **106**, 165131 (2022).

[58] S. Samanta, P. Detrattanawichai, S. Na-Phattalung, and H.-S. Kim, Active orbital degree of freedom and potential spin-orbit-entangled moments in the Kitaev magnet candidate $BaCo_2(AsO_4)_2$, Phys. Rev. B **106**, 195136 (2022).

[59] E. Rastelli, A. Tassi, and L. Reatto, Non-simple magnetic order for simple Hamiltonians, Physica B+C **97**, 1 (1979).

[60] J. B. Fouet, P. Sindzingre, and C. Lhuillier, An investigation of the quantum J1-J2-J3 model on the honeycomb lattice, The European Physical Journal B - Condensed Matter and Complex Systems **20**, 241 (2001).

[61] A. Mulder, R. Ganesh, L. Capriotti, and A. Paramekanti, Spiral order by disorder and lattice nematic order in a frustrated Heisenberg antiferromagnet on the honeycomb lattice, Phys. Rev. B **81**, 214419 (2010).

[62] R. Ganesh, D. N. Sheng, Y.-J. Kim, and A. Paramekanti, Quantum paramagnetic ground states on the honeycomb lattice and field-induced Néel order, Phys. Rev. B **83**, 144414 (2011).

[63] F. Mezzacapo and M. Boninsegni, Ground-state phase diagram of the quantum J_1-J_2 model on the honeycomb lattice, Phys. Rev. B **85**, 060402 (2012).

[64] R. Ganesh, J. van den Brink, and S. Nishimoto, Deconfined criticality in the frustrated Heisenberg honeycomb antiferromagnet, Phys. Rev. Lett. **110**, 127203 (2013).

[65] S. Pujari, K. Damle, and F. Alet, Néel-state to valence-bond-solid transition on the honeycomb lattice: Evidence for deconfined criticality, Phys. Rev. Lett. **111**, 087203 (2013).

[66] S.-S. Gong, D. N. Sheng, O. I. Motrunich, and M. P. A. Fisher, Phase diagram of the spin-$\frac{1}{2}$ J_1-J_2 Heisenberg model on a honeycomb lattice, Phys. Rev. B **88**, 165138 (2013).

[67] J. Carrasquilla, A. D. Ciolo, F. Becca, V. Galitski, and M. Rigol, Nature of the phases in the frustrated XY model on the honeycomb lattice, Phys. Rev. B **88**, 241109 (2013).

[68] A. Di Ciolo, J. Carrasquilla, F. Becca, M. Rigol, and V. Galitski, Spiral antiferromagnets beyond the spin-wave approximation: Frustrated XY and Heisenberg models on the honeycomb lattice, Phys. Rev. B **89**, 094413 (2014).

[69] Y. Huang, X.-Y. Dong, D. N. Sheng, and C. S. Ting, Quantum phase diagram and chiral spin liquid in the extended spin-$\frac{1}{2}$ honeycomb XY model, Phys. Rev. B **103**, L041108 (2021).

[70] P. A. Maksimov and A. L. Chernyshev, Easy-plane anisotropic-exchange magnets on a honeycomb lattice: Quantum effects and dealing with them, Phys. Rev. B **106**, 214411 (2022).

[71] E. R. Davidson, The iterative calculation of a few of the lowest eigenvalues and corresponding eigenvectors of large real-symmetric matrices, Journal of Computational Physics **17**, 87 (1975).

[72] E. R. Davidson and W. J. Thompson, Monster matrices: their eigenvalues and eigenvectors, Computers in Physics **7**, 519 (1993).

[73] C. W. Murray, S. C. Racine, and E. R. Davidson, Improved algorithms for the lowest few eigenvalues and associated eigenvectors of large matrices, Journal of Computational Physics **103**, 382 (1992).

[74] See Supplemental Material for details about (i) ED clusters and additional ED data and (ii) supporting DMRG data.

[75] S. R. White, Density matrix formulation for quantum renormalization groups, Phys. Rev. Lett. **69**, 2863 (1992).

[76] S. R. White, Density-matrix algorithms for quantum renormalization groups, Phys. Rev. B **48**, 10345 (1993).

[77] M. Kumar, Z. G. Soos, D. Sen, and S. Ramasesha, Modified density matrix renormalization group algorithm for the zigzag spin-$\frac{1}{2}$ chain with frustrated antiferromagnetic exchange: Comparison with field theory at large J_2/J_1, Phys. Rev. B **81**, 104406 (2010).

[78] U. Schollwöck, The density-matrix renormalization group, Rev. Mod. Phys. **77**, 259 (2005).

[79] V. J. Emery, E. Fradkin, S. A. Kivelson, and T. C. Lubensky, Quantum theory of the smectic metal state in stripe phases, Phys. Rev. Lett. **85**, 2160 (2000).

[80] A. Vishwanath and D. Carpentier, Two-dimensional anisotropic non-Fermi-liquid phase of coupled Luttinger liquids, Phys. Rev. Lett. **86**, 676 (2001).

[81] R. Mukhopadhyay, C. L. Kane, and T. C. Lubensky, Sliding Luttinger liquid phases, Phys. Rev. B **64**, 045120 (2001).

[82] O. A. Starykh, R. R. P. Singh, and G. C. Levine, Spinons in a crossed-chains model of a 2d spin liquid, Phys. Rev. Lett. **88**, 167203 (2002).

[83] P. Sindzingre, J.-B. Fouet, and C. Lhuillier, One-dimensional behavior and sliding Luttinger liquid phase in a frustrated spin-$\frac{1}{2}$ crossed chain model: Contribution of exact diagonalizations, Phys. Rev. B **66**, 174424 (2002).

[84] A. Bose, M. Routh, S. Voleti, S. K. Saha, M. Kumar, T. Saha-Dasgupta, and A. Paramekanti, Proximate dirac spin liquid in the j1-j3 xxz model for honeycomb cobaltates (2023), arXiv:2212.13271 [cond-mat.str-el].

[85] S. Jiang, S. R. White, and A. L. Chernyshev, Quantum phases in the honeycomb-lattice J_1–J_3 ferro-antiferromagnetic model (2023), arXiv:2304.06062 [cond-mat.str-el].

[86] Y. Watanabe, S. Trebst, and C. Hickey, Frustrated ferromagnetism of honeycomb cobaltates: Incommensurate spirals, quantum disordered phases, and out-of-plane Ising order (2022), arXiv:2212.14053 [cond-mat.str-el].

[87] F. Becca and S. Sorella, *Quantum Monte Carlo Approaches for Correlated Systems* (Cambridge University Press, 2017).

[88] I. Affleck, Z. Zou, T. Hsu, and P. W. Anderson, SU(2) gauge symmetry of the large-U limit of the Hubbard model, Phys. Rev. B **38**, 745 (1988).

[89] M. Hermele, SU(2) gauge theory of the Hubbard model and application to the honeycomb lattice, Phys. Rev. B **76**, 035125 (2007).

[90] N. Karthik and R. Narayanan, Scale-invariance and scale-breaking in parity-invariant three-dimensional QCD, Phys. Rev. D **97**, 054510 (2018).

[91] A. Thomson and S. Sachdev, Fermionic spinon theory of square lattice spin liquids near the Néel state, Phys. Rev. X **8**, 011012 (2018).

[92] A. M. Samarakoon, Q. Chen, H. Zhou, and V. O. Garlea, Static and dynamic magnetic properties of honeycomb lattice antiferromagnets $Na_2M_2TeO_6$, M = Co and Ni, Phys. Rev. B **104**, 184415 (2021).

[93] G. Xiao, Z. Xia, W. Zhang, X. Yue, S. Huang, X. Zhang, F. Yang, Y. Song, M. Wei, H. Deng, and D. Jiang, Crystal growth and the magnetic properties of $Na_2Co_2TeO_6$ with quasi-two-dimensional honeycomb lattice, Crystal Growth & Design **19**, 2658 (2019).